Catalysis Communications 143 (2020) 106046

Contents lists available at ScienceDirect

Catalysis Communications

journal homepage: www.elsevier.com/locate/catcom

Short communication

Mesoporous microspherical NiO catalysts for the deoxygenation of oleic acid

Courtney S. Smoljan[1], James M. Crawford[1], Moises A. Carreon*

Chemical & Biological Engineering Department, Colorado School of Mines, Golden, CO 80401, United States.

ARTICLEINFO

Keywords:
Mesoporous metal oxide
Biomass
Deoxygenation
Heterogeneous catalysis
Self-assembly

ABSTRACT

Mesoporous NiO catalysts were synthesized via surfactant assisted self-assembly employing structure directing agents CTAB and P123. The resultant catalysts had similar chemical composition but different physical properties including mesoporous ordering, surface area, and pore size. The mesoporous oxides were used as catalysts in the deoxygenation of oleic acid to heptadecane. The catalysts synthesized with P123 displayed the highest yields to heptadecane (63%) tripling the performance of commercial NiO (19%). A phase change from NiO to Ni was observed during the deoxygenation reaction. The recyclability of the catalyst synthesized with P123 was evaluated.

1. Introduction

Nickel based catalysts are known to be active catalytic phases for the deoxygenation of fatty acids to liquid fuel range hydrocarbons. Nickel is earth abundant and relatively inexpensive as compared to noble metals typically used for this reaction. The use of nickel for the deoxygenation of fatty acids to liquid fuel has been reported [1–6]. Miao et al. studied Ni/ZrO_2 catalysts under inert gas with the addition of water as the hydrogen donor [1]. These authors observed a yield of 64% and 47% to paraffin from oleic and stearic acid, respectively. Santillan-Jimenez et al. reported the deoxygenation of tristearin and stearic acid under a nitrogen atmosphere over Ni/C catalysts, and observed 81% and 19% conversion, respectively. The authors reported a selectivity for heptadecane of 75% and 50%, respectively [2]. The same research group studied Ni-Al layered double hydroxide catalysts for the same reaction, giving yields of 43% and 53% for tristearin and stearic acid, respectively [3]. Wu et al. studied the conversion of stearic acid over Ni/activated carbon and demonstrated nearly complete conversion and a selectivity to heptadecane of around 80% [4]. Song et al. explored the importance of synthesis methods comparing incipient wetness impregnated Ni/HBEA catalysts vs ion-exchanged catalysts. For the hydrodeoxygenation of stearic acid, these authors found that the ion-exchanged Ni/HBEA with a conversion of 97% outperformed the impregnated catalyst giving a conversion of only 33% [5]. Our group reported nickel-based metal organic frameworks supported on zeolites. We studied the decarboxylation of oleic acid and found a conversion of 92% and a heptadecane yield of up to 77% under CO_2 atmospheres [6]. Our group also recently reported the decarboxylation of Ni supported on zeolite mordenite with conversions of 54% and a yield to heptadecane of 47% under inert gas atmospheres [7]. The catalytic benefits of having hierarchically ordered pores for transition metal oxides in heterogeneous catalysis is well documented [8–11]. In particular, surfactant-assisted self-assembly approach represents a highly appealing method for the development of mesoporous transition metal oxide catalytic phases with desirable structural, compositional, and morphological properties [12–14]. Ordered pores in the mesoscale regime are highly desirable in catalysis to overcome potential mass transfer limitations due to pore restrictions. Herein, we demonstrate the successful synthesis of mesoporous nickel oxide via self-assembly approach and its use as efficient catalyst for the decarboxylation of oleic acid to heptadecane.

2. Experimental

2.1. Materials

Nickel (II) nitrate hexahydrate (98%, Sigma-Aldrich), Nickel (II) oxide (99.999% metal basis, Thermo-Fischer), hexadecyltrimethylammonium bromide (CTAB, 99%, Sigma-Aldrich), Pluronic P123 (P123, BASF), and ethanol (PharmCo, ACS reagent) were employed for the synthesis of mesoporous nickel oxide. Oleic acid (90%, Sigma-Aldrich) and n-hexane (99%, SupraSolv, Sigma-Aldrich) were used for deoxygenation experiments. N,O-Bis(trimethylsilyl)triflouroacetamide (BTSFA, 99%, ACS reagent, Sigma-Aldrich) was employed for GC–MS analysis. Potassium bromide (KBr, 99.99%, Arcos) was used to generate infrared sample pellets. Methanol (PharmCo, ACS reagent)

* Corresponding author.
E-mail address: mcarreon@mines.edu (M.A. Carreon).
[1] These authors contributed equally to this work.

https://doi.org/10.1016/j.catcom.2020.106046
Received 28 March 2020; Received in revised form 8 May 2020; Accepted 11 May 2020
Available online 15 May 2020

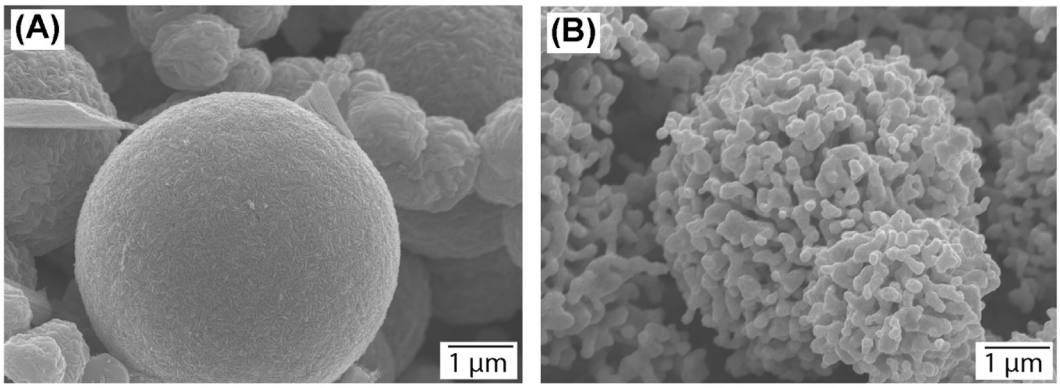

Fig. 1. SEM images of fresh P123 (A) and recycled P123 (B).

was used to rinse the catalyst.

2.2. Catalyst synthesis

NiO powder was crushed and sieved to a particle size between 150 and 250 μm providing the 'NiO powder' catalyst. To synthesize mesoporous NiO, we employed the surfactant self-assembly approach. Nickel (II) nitrate hexahydrate was used as the inorganic precursor, while P123 and CTAB were used as structure directing agents (SDA), and ethanol was used as the solvent. The SDA solution was prepared by adding 0.973 g of P123 or 0.501 g of CTAB to 11.407 g of solvent and stirring for few minutes at 60 °C until a homogenous solution formed [15]. The precursor solution was prepared by adding 8.0 g of nickel (II) nitrate hexahydrate to 11.407 g of solvent and stirring at 60 °C until homogenous. The SDA solution was then added dropwise to the precursor solution and stirred at approximately 60 °C for 30 min. The resulting gel was transferred to a Teflon lined autoclave and heated to 150 °C for 20 h (10 °C/min ramp). The cooled product was centrifuged for 20 min at 4000 rpm and washed three times with ethanol before it was dried overnight at 85 °C. To remove the SDA, the catalysts were calcined at 320 °C for 12 h (1 °C/min ramp). The obtained catalysts were named according to the SDA used in the synthesis as 'P123' and 'CTAB' NiO catalysts.

2.3. Deoxygenation experiments

In a typical deoxygenation experiment, 250 mg of NiO catalyst, 1000 mg of oleic acid, and 10 ml of hexane were loaded into a 100 ml batch reactor (Parr, Model 4560). The reactor was flushed with hydrogen five times, sealed, and pressurized at 20 bar H_2. The reactor was heated to 300 °C and held for 3 h while stirring at 600 rpm. The reaction was determined to be kinetically limited by calculating the Thiele modulus (Table S1). When the reaction was completed, the reactor was allowed to cool to room temperature and the resultant liquid product was analyzed. Separation of the catalyst from the reaction mixture was accomplished using a magnet, owing to the unique magnetic properties of Ni. The catalyst was rinsed with hexane 3 times and methanol 3 times, dried overnight at 70 °C under vacuum, and either collected for analysis of the recycled catalyst or exposed to an additional reaction.

2.4. Catalyst characterization

The resultant catalysts, denoted with respect to the surfactant used in their synthesis, were characterized and compared vs commercially available NiO for the deoxygenation of oleic acid. Small angle x-ray scattering (SAXS, Anton Paar SAXSess, 25 mA, 30 kV, Cu Kα) was employed to confirm the existence of the mesostructure in the catalyst. The crystal structure and crystallite size (Scherrer equation) were inspected by powder X-ray diffraction (PXRD, Siemens, Kristalloflex800, 25 mA, 30 kV, Cu Kα). Nitrogen physisorption isotherms were collected at 77 K (ASAP 2020, Micrometrics) providing the Brunauer-Emmett-Teller (BET) surface area, pore volume (t-plot method) and Barrett-Joyner-Halenda (BJH) pore size distributions calculated from the desorption branch. All samples were degassed at 300 °C under high vacuum for 5 h prior to collecting the isotherms. Residual SDA, coke content, and the effect of calcination was measured by thermogravimetric analysis (TGA, TA Instruments). TGA was conducted under argon flow with a ramp rate of 10 °C/min. Field emission scanning electron microscopy (FE-SEM) images of the catalyst morphology were collected using an accelerating voltage of 5 kV (JEOL-ISM-7000F).

2.5. Liquid product analysis

After the reactor cooled to room temperature, all reaction products were collected in a 15 ml falcon tube. The sample was vortexed and sonicated to form a homogeneous solution. Hexane (600 μl), liquid sample (300 μl), and BTSFA (30 μl) were combined in a 2 ml GC vial and subject to heating (60 °C) for 1 h to allow complete silylation of the fatty acids. Following, 0.2 μl of the sample was injected (Agilent AS, 7683B) on to a gas chromatograph (Agilent GC, 6980N), separated by a HP-5 MS column (30 m × 250 μm × 0.25 μm), heated (5 °C/min ramp rate from 40 °C to 250 °C hold for 10 min), and detected by MS (Agilent MSD, 5973N).

3. Results and discussion

3.1. Catalyst characterization

Scanning electron microscopy (SEM) images showed distinctive micron scale spherical morphologies in both the fresh P123 (Fig. 1A) and fresh CTAB (Fig. S1). The microspheres exhibited some polydispersity and yielded an average particle size of 3.18 ± 1.33 and 3.45 ± 1.22 μm for CTAB and P123, respectively (Fig. S2). Higher magnification of the particles revealed a flower-petal like morphology on the surface of the spheres. A similar spherical morphology has been observed for mesoporous gallium oxides [15]. The recycled P123 catalyst is discussed in detail in the Catalyst Recyclability section below.

Nitrogen physisorption isotherms confirmed that the NiO powder (Fig. 2) did not exhibit strong nitrogen uptakes. CTAB and P123 samples indicated Type IV isotherms typical of mesoporous materials. The pore size distribution, calculated from the desorption branch, using the BJH method, displayed a minimal presence of pores in the NiO powder. The CTAB sample had a large hysteresis loop, which was indicative of condensation in the mesopores. The same was observed in the P123 sample, but with a higher uptake of N_2 at low pressures. The CTAB and P123 samples gave an average pore size of 4.9 and 3.9 nm, respectively.

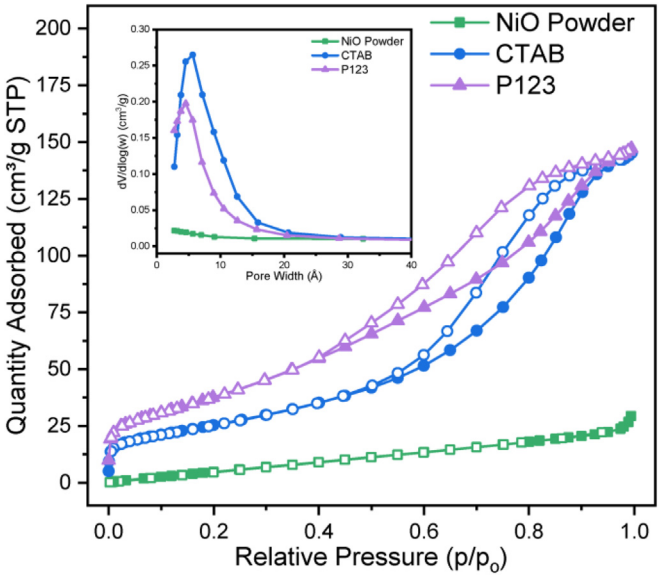

Fig. 2. N $_2$-isotherms (77 K) of NiO powder (square), CTAB (circle), and P123 (triangle). Insets provide the average pore diameter calculated from the desorption branch using the BJH method.

Table 1
Textural properties of the fresh and recycled catalysts.

Sample	S_{BET} [a]	V_{meso} [b]	D_{pore} [b]	D_{crys} [c]	D_{part} [d]
	(m^2/g)	(cm^3/g)	(nm)	(nm)	(μm)
NiO powder	32.6	0.03	–	35.8	n/a
CTAB	91.9	0.16	4.9	7.8	3.18 ± 1.33
P123	137.7	0.14	3.9	5.2	3.45 ± 1.22
P123 recycle	112.6	0.09	–	37.3	n/a

[a] Surface area (S_{BET}) was calculated using the BET method.
[b] Mesopore volume (V_{meso}) and pore diameter (D_{pore}) were calculated by the BJH desorption method.
[c] Crystallite size (D_{cryst}) was calculated using the Scherrer equation.
[d] Particle size (D_{part}) was measured by SEM image analysis (n = 250).

Surface area, mesopore volume, crystallite size, and particle size are shown in Table 1. Clearly, P123 gave the highest surface area followed by CTAB: 137.7 m^2/g and 91.9 m^2/g, respectively.

Fresh catalysts were characterized using small angle X-ray scattering (SAXS) to elucidate the formation of the mesostructures (Fig. S3). The commercial NiO powder did not exhibit the formation of a mesostructure, as indicated by the absence of any reflection or shoulder at low 2θ and corroborated by the N $_2$-isotherms. The CTAB and P123 samples displayed a broad shoulder between 2θ = 1–1.5°, indicative of a wormhole disordered mesostructures [15]. At higher angles, characterized by powder X-ray diffraction (PXRD), all fresh samples displayed the same face-centered cubic NiO structure (Fig. 3) with characteristic reflections occurring at 2θ = 37.2° and 43.2° (JCPDS #47-1049). The NiO powder, as received, showed a metallic Ni phase impurity at 2θ = 44.5° (JCPDS #87-0712). This Ni phase impurity made up less than 5% of the composition, as determined by area comparison of the NiO and Ni reflections.

To better understand the thermal stability of the catalysts and to guide our calcination approach, TGA was carried out. NiO exhibited no evident weight loss (Fig. S4). In the case of the mesoporous samples, we found that the initiation of SDA removal in uncalcined CTAB and P123 was around 300 °C. SDA removal was complete at ~400 °C in both samples. Based on this TGA analysis, we calcined both CTAB and P123 at 320 °C for 12 h using a slow ramp of 1 °C/min. After calcination, we found that both CTAB and P123 had only 4% and 5% of the SDA remaining, respectively, indicated by the weight loss in the thermograms (Fig. S4).

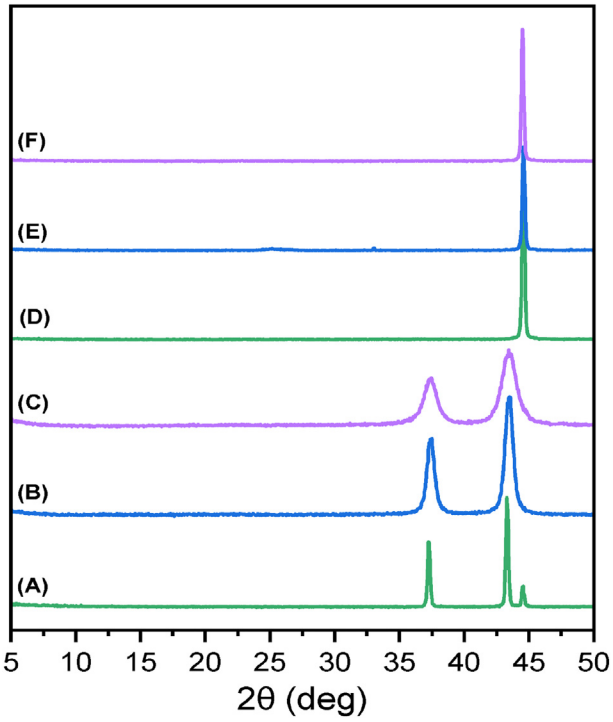

Fig. 3. PXRD for fresh NiO powder (A), fresh CTAB (B), fresh P123 (C), recycled NiO powder (D), recycled CTAB (E), and recycled P123 (F) catalysts.

3.2. Catalytic deoxygenation results

The similarity in the composition of all studied NiO catalysts provided insights into the mechanistic deoxygenation of oleic acid. Primary deoxygenation pathways that have been reported for oleic acid and other fatty acid methyl esters include hydrodeoxygenation (HDO), decarboxylation (DCO), and decarbonylation (DCN). Each pathway has previously been described in detail [16,17]. Products formed from oleic acid that are indicative of the HDO pathway are stearic acid (SA) and octadecane (C_{18}). Heptadecane (C_{17}) and shorter n-alkanes are indicative of the DCO pathway. Alkenes are evidence of the DCN pathway. The reaction products (Table 2) indicate that the NiO powder promoted both HDO and DCO pathways with the primary reaction product being SA. The average C_{17} yield for the NiO powder catalyst was only 19.1%. Some of the alkane products were cracked to light hydrocarbons (C_{11}-C_{16}). No alkenes were observed in the NiO powder reaction indicating that DCN was not promoted. The only other products observed for the NiO powder was hepta- and hexadecanoic acid.

Table 2
Products from the deoxygenation of oleic acid with NiO catalysts.

Catalyst	Yield (mol %)							X (%)
	C_{11}-C_{16}	C_{17}-ene	C_{17}	C_{18}-ene	C_{18}	SA	Other	
NiO powder	0.6	–	16.7	–	8.5	71.9	2.3	100.0
NiO powder	1.6	–	21.5	–	7.0	61.7	2.1	100.0
CTAB	1.0	10.5	11.3	4.7	7.7	42.3	18.2	95.7
CTAB	0.4	15.2	11.4	5.2	6.0	37.7	20.4	96.3
P123	15.5	–	61.3	–	7.0	14.3	1.9	100.0
P123	4.8	–	64.8	–	6.8	23.5	1.2	100.0
P123 recycle	–	–	35.3	–	10.3	52.2	1.9	100.0

Reaction Conditions: Catalyst: Oleic = 1:4 (mg), P = 20 bar H_2, T = 300 °C, t = 3 h, ω = 600 rpm, solvent = hexane (10 ml).

Table 3
Comparison of the state-of-the-art Ni based catalysts for the deoxygenation of oleic acid to heptadecane.

Ref.	Catalyst	Reaction conditions				X (%)	C_{17} Yield (%)
		T (°C)	P (bar)	t (min)	Gas		
[25]	Ni/MgO-Al_2O_3	280	35	360	H_2	100	26
[25]	Ni/CaO-Al_2O_3	280	35	360	H_2	100	10
[25]	Ni/NiO-Al_2O_3	280	35	360	H_2	100	94
[25]	Ni/CuO-Al_2O_3	280	35	360	H_2	100	95
[25]	Ni/ZnO-Al_2O_3	280	35	360	H_2	100	95
[26]	Ni-CZO	300	1	180	H_2/N_2	98	14
[27]	Ni/MgO-Al_2O_3	300	1	180	N_2	31	2
[28]	Ni-Cu/ZrO_2	330	a	180	a	100	35
[29]	Ni/Mo-Al_2O_3	330	40	1440	N_2	96	55
[30]	Ni/C	350	a	240	a	100	41
[31]	Ni/HZSM-5	360	40	300	H_2	100	44
This work	P123	300	20	180	H_2	100	63

Microbatch reactor experiments without gas atmosphere control.

CTAB catalysts promoted HDO, DCO, and DCN pathways with an average yield to C_{17} of 11.4%. The abundance of competitive reactions resulted in a lower selectivity to desired long-chain alkanes. Other side products from the CTAB sample reaction included light alkenes, cyclohexane, and aromatic products. These products are indicative of both cracking and Diels-Alder reaction pathways [18]. Ni is a known hydrocracking catalyst [19]. We suggest that the larger pore size in the CTAB catalysts (4.9 nm) as compared to P123 catalysts (3.9 nm) allowed facile desorption of various reaction products, therefore promoting in principle additional pathways. Additionally, the polymerization of cracking products could deactivate the surface and explain the lower conversion and slightly higher coking on the CTAB catalyst as compared to P123. The P123 catalysts promoted the DCO pathway with an average C_{17} yield of 63.1%. Also in high abundance was SA which was a result of the HDO pathway. Some shorter n-alkanes were also observed for the P123 catalyst. The only other product observed for P123 was heptadecanoic acid. Overall, P123 was a highly active catalyst for the conversion of oleic acid to n-heptadecane. The higher surface area and enhanced local structural order (assessed by the more pronounced broad peak at 2theta ~ 1.5) may be responsible for the improved catalytic performance of P123 catalyst to n-heptadecane as compared to CTAB catalyst. No DCN products were observed in the P123 catalyst. Representative GC–MS are provided in Fig. S5.

3.3. Catalyst recyclability

The recycled catalysts were characterized by SEM, PXRD, and TGA. As shown in Fig. 1B, the recycled P123 exhibited changes from microspheres to a skeletal coral like morphology. This was likely a product of the hydrogen atmosphere in the reactor, promoting the reduction of NiO to Ni. This claim was corroborated by PXRD as indicated by the reflection at $2\theta = 44.5°$ (Fig. 2) and the magnetic behavior of the sample (Fig. S6, Video S1). The reduction of NiO to Ni^0 has been previously reported using temperature programmed reduction, where it was determined that unsupported NiO was fully reduced at temperatures above 220 °C [20]. The narrowed full width half maximum of the spent catalysts indicates that the small crystallites agglomerated (Table 1) in agreement with observations in SEM. TGA was conducted on the spent catalysts to measure the accumulation of organic and carbonaceous coke compounds. This analysis revealed that the CTAB and P123 samples accumulated ~2.5 wt% and ~1.5 wt% coke, respectively (Fig. S4). P123 was selected for a second reaction owing to the high performance as a fresh catalyst, the limited coke residues, and the retention of active surface area. After rinsing with hexane and methanol and drying overnight under vacuum at 70 °C, the recycled P123 was exposed to a second reaction. The primary products from the recycled P123 reaction were stearic acid (52.2%), C_{17} (35.3%), and C_{18} (10.3%) indicating that HDO and DCO pathways remained dominant. Interestingly, the loss of the short n-alkanes as products suggests that the elimination of small pores (3.9 nm), evidenced in the isotherms, prevented further carbon-carbon bond breakage, which can be promoted by Ni catalysts [19]. The combined yield for C_{17} and C_{18} hydrocarbons went from 70.0% to 45.8% in the fresh and recycled P123, respectively. In general, the recycled P123 products were similar to that of the NiO powder, but with a higher yield of C_{17}. While the activity of the recycled P123 catalyst was significantly lower than the fresh catalyst, the yield to heptadecane remained higher than the fresh commercial NiO powder and fresh CTAB catalysts. Additionally, the conversion of oleic acid remained complete, with no reactant in the final product mixture. We can conclude from our analysis, that the presence of a mesopore on similar scales with the reactant molecule can promote different reaction pathways and provide high yields to C_{17}.

3.4. Comparison to the state-of-the-art

Previously reported catalyst systems and the use of non-noble metals including Ni for the deoxygenation of bio-derived fatty acids has been reviewed [16,21]. Key reaction parameters in the deoxygenation of oleic acid are temperature, pressure, reaction time, and gas atmosphere. It has been shown that under sufficient H_2 pressure, complete conversion of oleic acid is often observed. Additionally, by increasing the pressure of H_2 an optimal yield of C_{17} can be accomplished. Operating at high H_2 pressures also has a trade-off with respect to process safety and the efficiency of the process [22–24]. Our work highlights the possibility of utilizing a facile synthesis, moderate reaction conditions, and a single component catalyst that provides competitive conversion and selectivity to C_{17}. In comparison to the state-of-the-art Ni-based catalysts [25–31], the fresh P123 catalyst provides high yields to C_{17} (Table 3). While few reports document higher C_{17} yields, significantly higher H_2 pressures and longer reaction times are needed. Additionally, our work characterizes the recycled catalyst, providing evidence that the loss of mesoporosity results in lower C_{17} yields.

4. Conclusion

In summary, we have reported NiO based catalysts with disordered wormhole mesoporosity. An in situ reduction of the NiO occurred during the reaction with oleic acid, evidenced by the change in crystal phase. In comparison to commercial NiO powder (C_{17} yield = 19%), the P123 catalyst led to the highest conversion (100%) and yield (63%) to C_{17}. In contrast, the CTAB catalyst with larger mesopore promoted additional deoxygenation pathways including HDO, DCO, and DCN. As a result, lower yields to C_{17} were observed (11%).The enhanced catalytic activity of the P123 catalyst was attributed to the high surface

area, mesopores, and limited coking. Upon recycling, the P123 catalyst showed a decrease in C_{17} yield to ~35%. Nevertheless, the fresh mesoporous P123 catalyst displayed > 3 times higher yield to C_{17} as compared to commercially available NiO, and about twice the yield to C_{17} after recycling. The primary pathway observed in the P123 catalyst was HDO and DCO.

Supplementary data to this article can be found online at https://doi.org/10.1016/j.catcom.2020.106046.

Author statement

M.A.C. conceptualization, funding acquisition, supervision. C.S.S. and J.M.C. Investigation and Formal analysis.

Declaration of Competing Interest

The authors declare that they have no known competing financial interests or personal relationships that could have appeared to influence the work reported in this paper.

Acknowledgements

J.C. thanks the National Science Foundation Graduate Research Fellowship Program NSF-GRFP for financial support of this work. M.C. thanks the National Science Foundation NSF-CBET Award # 1705675 for supporting this work financially. C.S. thanks Colorado School of Mines MURF fellowship.

References

[1] C. Miao, O. Marin-flores, T. Dong, D. Gao, Y. Wang, M. Garcia-pe, S. Chen, Hydrothermal Catalytic Deoxygenation of Fatty Acid and Bio-oil With In Situ H, 2 (2018), pp. 2–11, https://doi.org/10.1021/acssuschemeng.7b02226.

[2] E. Santillan-Jimenez, T. Morgan, J. Lancy, S. Mohapatra, M. Crocker, Catalytic deoxygenation of triglycerides and fatty acids to hydrocarbons over carbon-supported nickel, Fuel. 103 (2013) 1010–1017, https://doi.org/10.1016/j.cattod.2013.11.009.

[3] E. Santillan-Jimenez, T. Morgan, J. Shoup, A.E. Harman-Ware, M. Crocker, Catalytic deoxygenation of triglycerides and fatty acids to hydrocarbons over Ni–Al layered double hydroxide, Catal. Today 237 (2014) 136–144, https://doi.org/10.1016/J.CATTOD.2013.11.009.

[4] J. Wu, J. Shi, J. Fu, J.A. Leidl, Z. Hou, X. Lu, Catalytic decarboxylation of fatty acids to aviation fuels over nickel supported on activated carbon, Sci. Rep. 6 (2016) 27820, https://doi.org/10.1038/srep27820.

[5] W. Song, C. Zhao, J.A. Lercher, Importance of size and distribution of Ni nanoparticles for the hydrodeoxygenation of microalgae oil, Chem. Eur. J. 19 (2013) 9833–9842, https://doi.org/10.1002/chem.201301005.

[6] L. Yang, B.W. McNichols, M. Davidson, B. Schweitzer, D.A. Gómez-Gualdrón, B.G. Trewyn, A. Sellinger, M.A. Carreon, Noble metal-free catalytic decarboxylation of oleic acid to n-heptadecane on nickel-based metal-organic frameworks (MOFs), Catal. Sci. Technol. 7 (2017) 3027–3035, https://doi.org/10.1039/c7cy00564d.

[7] J.M. Crawford, S.F. Zaccarine, N.C. Kovach, C.S. Smoljan, J. Lucero, B.G. Trewyn, S. Pylypenko, M.A. Carreon, Decarboxylation of stearic acid over Ni/MOR catalysts, J. Chem. Technol. Biotechnol. (2019), https://doi.org/10.1002/jctb.6211.

[8] Y. Rao, D.M. Antonelli, Mesoporous transition metal oxides: characterization and applications in heterogeneous catalysis, J. Mater. Chem. 19 (2009) 1937–1944, https://doi.org/10.1039/b813533a.

[9] A. Taguchi, F. Schüth, Ordered mesoporous materials in catalysis, Microporous Mesoporous Mater. 77 (2005) 1–45, https://doi.org/10.1016/J.MICROMESO.2004.06.030.

[10] M.A. Carreon, V.V. Guliants, L. Yuan, A.R. Hughett, A. Dozier, G.A. Seisenbaeva, V.G. Kessler, Mesoporous nanocrystalline mixed metal oxides from heterometallic alkoxide precursors: cobalt-nickel oxide spinels for propane oxidation, Eur. J. Inorg. Chem. (2006) 4983–4988, https://doi.org/10.1002/ejic.200600747.

[11] M.A. Carreon, V.V. Guliants, Macroporous vanadium phosphorus oxide phases displaying three-dimensional arrays of spherical voids, Chem. Mater. 14 (2002) 2670–2675, https://doi.org/10.1021/cm0117376.

[12] M.E.R.W.J.V.J.C, B.J.S. Kresge, C.T. Leoniwicz, Ordered mesoporous molecular synthesized by a liquid-crystal template, Lett. To Nat. 359 (1992) 710–712.

[13] J.S. Beck, J.C. Vartuli, W.J. Roth, M.E. Leonowicz, C.T. Kresge, K.D. Schmitt, C.T.W. Chu, D.H. Olson, E.W. Sheppard, S.B. McCullen, J.B. Higgins, J.L. Schlenker, A new family of mesoporous molecular sieves prepared with liquid crystal tmeplates, J. Am. Chem. Soc. 114 (1992) 10834–10843, https://doi.org/10.1021/ja00053a020.

[14] M.A. Carreon, V.V. Guliants, Ordered meso- and macroporous binary and mixed metal oxides, Eur. J. Inorg. Chem. 2005 (2005) 27–43, https://doi.org/10.1002/ejic.200400675.

[15] C.A. Deshmane, J.B. Jasinski, M.A. Carreon, Thermally stable nanocrystalline mesoporous gallium oxide phases, Eur. J. Inorg. Chem. 2009 (2009) 3275– 3281, https://doi.org/10.1002/ejic.200900359.

[16] R.W. Gosselink, S.A.W. Hollak, S.W. Chang, J. Van Haveren, K.P. De Jong, J.H. Bitter, D.S. Van Es, Reaction pathways for the deoxygenation of vegetable oils and related model compounds, ChemSusChem. 6 (2013) 1576–1594, https://doi.org/10.1002/cssc.201300370.

[17] L. Yang, M.A. Carreon, Deoxygenation of palmitic and Lauric acids over Pt/ZIF-67 membrane/zeolite 5A bead catalysts, ACS Appl. Mater. Interfaces 9 (2017) 31993–32000, https://doi.org/10.1021/acsami.7b11638.

[18] R.O. Idem, S.P.R. Katikaneni, N.N. Bakhshi, Catalytic conversion of canola oil to fuels and chemicals: roles of catalyst acidity, basicity and shape selectivity on product distribution, Fuel Process. Technol. 51 (1997) 101–125, https://doi.org/10.1016/S0378-3820(96)01085-5.

[19] J.G. Speight, Refining chemistry and fouling potential, Fouling in Refineries, Elsevier, 2015, pp. 65–86, , https://doi.org/10.1016/B978-0-12-800777-8.00003-6.

[20] C. Li, Y.-W. Chen, Temperature-programmed-reduction studies of nickel oxide/alumina catalysts: effects of the preparation method, Thermochim. Acta 256 (1995) 457–465, https://doi.org/10.1016/0040-6031(94)02177-P.

[21] A. Kiméné, R. Wojcieszak, S. Paul, F. Dumeignil, Catalytic decarboxylation of fatty acids to hydrocarbons over non-noble metal catalysts: the state of the art, J. Chem. Technol. Biotechnol. (2018), https://doi.org/10.1002/jctb.5776.

[22] J.M. Crawford, M.A. Carreon, Decarboxylation of diunsaturated linoleic acid to heptadecane over zeolite supported Pt/ZIF-67 catalysts, Ind. Eng. Chem. Res. 57 (2018) 15991–15997, https://doi.org/10.1021/acs.iecr.8b02799.

[23] J.M. Crawford, C.S. Smoljan, J. Lucero, M.A. Carreon, Deoxygenation of stearic acid over cobalt-based NaX zeolite catalysts, Catalysts. 9 (2019) 42, https://doi.org/10.3390/catal9010042.

[24] J. Zhang, C. Zhao, Development of a bimetallic Pd-Ni/HZSM-5 catalyst for the tandem limonene dehydrogenation and fatty acid deoxygenation to alkanes and arenes for use as biojet fuel, ACS Catal. 6 (2016) 4512–4525, https://doi.org/10.1021/acscatal.6b00520.

[25] G. Li, F. Zhang, L. Chen, C. Zhang, H. Huang, X. Li, Highly selective hydrodecarbonylation of oleic acid into n-heptadecane over a supported nickel/zinc oxide-alumina catalyst, ChemCatChem. 7 (2015) 2646–2653, https://doi.org/10.1002/cctc.201500418.

[26] K.-W. Jeon, J.-O. Shim, W.-J. Jang, D.-W. Lee, H.-S. Na, H.-M. Kim, Y.-L. Lee, S.-Y. Yoo, H.-S. Roh, B.-H. Jeon, J.W. Bae, C.H. Ko, Effect of calcination temperature on the association between free NiO species and catalytic activity of Ni−Ce0.6Zr0.4O2 deoxygenation catalysts for biodiesel production, Renew. Energy 131 (2019) 144–151, https://doi.org/10.1016/j.renene.2018.07.042.

[27] H.-S. Roh, I.-H. Eum, D.-W. Jeong, B.E. Yi, J.-G. Na, C.H. Ko, The effect of calcination temperature on the performance of Ni/MgO–Al2O3 catalysts for decarboxylation of oleic acid, Catal. Today 164 (2011) 457– 460, https://doi.org/10.1016/j.cattod.2010.10.048.

[28] Z. Zhang, H. Chen, C. Wang, K. Chen, X. Lu, P. Ouyang, J. Fu, Efficient and stable Cu-Ni/ZrO2 catalysts for in situ hydrogenation and deoxygenation of oleic acid into heptadecane using methanol as a hydrogen donor, Fuel. 230 (2018) 211–217, https://doi.org/10.1016/j.fuel.2018.05.018.

[29] N. Krobkrong, V. Itthibenchapong, P. Khongpracha, K. Faungnawakij, Deoxygenation of oleic acid under an inert atmosphere using molybdenum oxide-based catalysts, Energy Convers. Manag. 167 (2018) 1–8, https://doi.org/10.1016/j.enconman.2018.04.079.

[30] Z. Zhang, Z. Chen, X. Gou, H. Chen, K. Chen, X. Lu, P. Ouyang, J. Fu, Catalytic decarboxylation and aromatization of oleic acid over Ni/AC without an added hydrogen donor, Ind. Eng. Chem. Res. 57 (2018) 8443–8448, https://doi.org/10.1021/acs.iecr.8b01768.

[31] S. Xing, P. Lv, C. Zhao, M. Li, L. Yang, Z. Wang, Y. Chen, S. Liu, Solvent-free catalytic deoxygenation of oleic acid via nano-Ni/HZSM-5: effect of reaction medium and coke characterization, Fuel Process. Technol. 179 (2018) 324–333, https://doi.org/10.1016/j.fuproc.2018.07.024.